# Compact Metamaterial-Based UHF RFID Antennas: Deformed Omega and Split-Ring Resonator Structures

**Benjamin D. Braaten[1], Robert P. Scheeler[1], Michael Reich[2], Robert M. Nelson[3], Cherish Bauer-Reich[4], Jacob Glower[1] and Gregory J. Owen[1]**

[1] Department of Electrical and Computer Engineering
North Dakota State University, Fargo, ND, 58102, USA
benbraaten@ieee.org

[2] Center for Nanoscale Science and Engineering (CNSE)
North Dakota State University, Fargo, ND, 58102, USA

[3] Engineering and Technology Department
University of Wisconsin - Stout, Menomonie, WI, 54751, USA

[4] Department of Geology and Geophysics
University of Minnesota – Twin Cities, Minneapolis, MN, USA

***Abstract –*** Over the past decade, researchers have shown significant advances in the area of radio frequency identification (RFID) and metamaterials. RFID is being applied to a wide spectrum of industries and metamaterial-based antennas are beginning to perform just as well as existing larger printed antennas. This paper presents two novel metamaterial-based antennas for passive ultra-high frequency (UHF) RFID tags. It is shown that by implementing omega-like elements and split-ring resonators into the design of an antenna for an UHF RFID tag, the overall size of the antenna can be significantly reduced to dimensions of less than $0.15\lambda_0$, while preserving the performance of the antenna.

***Index Terms-*** Metamaterial, RFID, meander-line, split-ring resonator, printed antenna, passive tag.

## I. INTRODUCTION

The use of radio frequency identification (RFID) has grown substantially in recent years [1-4]. RFID has been applied to many different industries such as supply chain management [5], disease prevention [6-7], security [8] and road-tolling [9]. Because of these applications significant research is being conducted in the areas of antenna design [10], environmental effects on RFID systems [11] and novel reader applications [12].

The two major characteristics that distinguish different types of RFID systems are the power source of the tag and the frequency of operation [1]. An excellent review on the characteristics of different types of RFID systems can be found in [1]. A passive RFID system uses the energy from the field radiated by the reader to completely power the tags. A tag in this type of system usually has an antenna attached to a rectifier circuit. This rectifier circuit then provides a voltage and current that will be used to power the tag circuitry. At Ultra-high frequencies (UHF) it is the relation between the input impedance of the rectifier circuit and the antenna impedance and gain that will determine the maximum read range of the tag [6], [10].

When designing a passive RFID tag, it is clear that the antenna is a major component of the overall size [6]. This is because it is difficult to attain an inductive input reactance and a suitable gain of an electrically small antenna. A new and rapidly emerging field of research based on metamaterial inspired antennas [13-16] is showing that antennas with small physical size can have impedance and radiation properties comparable to existing larger antennas such as rectangular microstrip and meander-line (space-filling) antennas. In particular research in the area of metamaterials has resulted in recent advances in optics [17], filters [18], novel resonator structures [19-20], novel transmission lines [21-23] and new compact power dividers [24].

Many advances in metamaterial research have represented very significant steps in the area of antenna and microwave engineering. But, many of the structures introduced so far are very complicated, and in some cases this is a significant drawback. When designing metamaterial- based antennas, many different conducting planes, vias and special ground planes are required. These complicated structures are not easily applied to passive RFID antenna designs. This is because many passive RFID antenna designs are placed on single conducting layers with one or two different dielectric layers. In fact, very little work exists on strictly planar-based metamaterial transmission lines [25].

Recently, several initial studies have been conducted on using metamaterials to enhance the performance of passive RFID tags [26-27]. These studies have shown promising results but several drawbacks of these studies have also been observed. For example, the designs are placed above special ground planes, the feed networks can be complicated and a clear design process for using these antennas is not presented. Since typical antennas printed on passive RFID tags are placed on a single conducting layer, it may be desirable not to have a ground plane, have a simple feed network and have a very useful and clear set of design guidelines to result in a simple and desirable printed antenna.

In this paper, two different metamaterial-based designs for passive UHF RFID antennas are presented. The first design is based on the deformed omega structure presented in [28] and the second design is based on the split-ring resonator structure (SRR) [29]. Several advantages of the designs presented in this paper are that these antennas 1) do not need a ground plane; 2) are on a single conducting layer; 3) have a single dielectric substrate; 4) have simple feed networks; 5) are up to 50% smaller than commercially available passive RFID tags; 6) are comparable to the performance of commercially available passive RFID tags; 7) are simple to design; and 8) are easy to manufacture. Many different layouts with different material properties are studied. These different cases are extensive and presented here to clearly show how various dimensions and substrate values can be used to lead to a successful antenna design. It is believed that by using the results presented in this

paper, an antenna designer will avoid costly simulation times as well as less than desirable performance from manufactured antennas. This is especially important during the usually extensive antenna design process.

This paper is organized in the following manner. Section II introduces the deformed omega structure-based meander-line RFID antenna. Within this section simulations from commercial software are compared to measurements for accuracy and various configurations of the printed antenna are modeled to illustrate the characteristics of the antenna. Section III introduces the SRR-based RFID antenna. Within this section various configurations are modeled with commercial software and the characteristics of these designs are presented. These sections are followed by a conclusion in section IV.

## II. DEFORMED OMEGA STRUCTURE-BASED MEANDER-LINE RFID ANTENNA

### A. The Three Different Meander-Line Geometries

The first antenna presented is a meander-line antenna with metamaterial elements. These elements are based on the left-handed deformed omega structure presented in [28]. A typical element of a deformed omega structure is shown in Fig. 1. Several meander-line sections are also shown with s denoting the trace width, a denoting the element width, k denoting the width between the traces, p denoting the trace width of the deformed omega element, m denoting the overall width of the antenna, $\Delta$ denoting the height of the deformed omega element and $\delta$ denoting the height of the meander-line sections.

Three different versions of the antenna in Fig. 1 were evaluated. These three versions are shown in Fig. 2. Fig. 2 (a) is the meander-line antenna with zero (N = 0) deformed omega elements, Fig. 2 (b) is the meander-line antenna with two (N = 2) deformed omega elements and Fig. 2 (c) is the meander-line antenna with four (N = 4) deformed omega elements. These three different designs were studied to determine how the introduction of the deformed omega elements into the meander-line layout would affect the input impedance and gain of the antenna. This information provides useful guidelines for antenna designers.
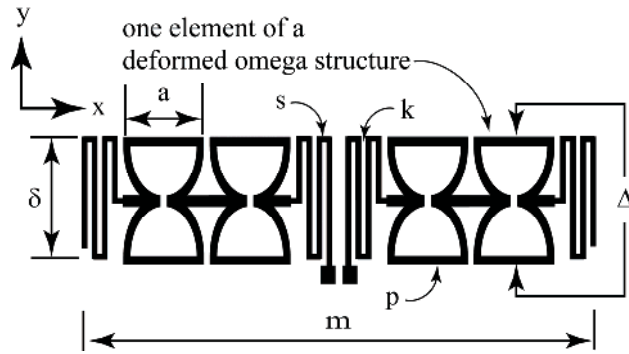
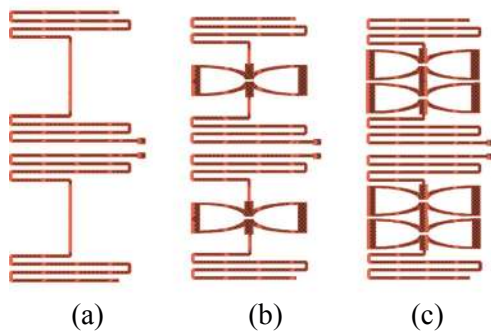Fig. 1. Deformed omega structure-based meander-line RFID antenna dimensions [28].



Fig. 2. (a) Layout of the omega structure with no deformed omega elements (N = 0); (b) layout of the omega structure with two deformed omega elements (N = 2); (c) layout of the omega structure with four deformed omega elements (N = 4).

## B. Validation of the Numerical Results with Measurements

The first step in modeling the antennas in this paper was to compare the simulated values with measurements. To do this, the printed antenna in Fig. 3 was manufactured on FR4 ($\varepsilon_r$ = 3.75 measured) with a thickness of d = 0.787 mm. The input impedance was measured with a network analyzer in an anechoic chamber (Fig. 4) using a balanced probe [30] and was compared to the simulation results from the commercial software Advanced Design System (ADS) [31] by Agilent Technologies. The results from these measurements and simulations are shown in Fig. 5 (a). Figure 5 shows good agreement between the measurements and simulations. The magnitude of the electric field in the y-z and x-z planes is also shown in Fig. 5 (b) and (c), respectively, along with the simulated current distribution in part (d). This
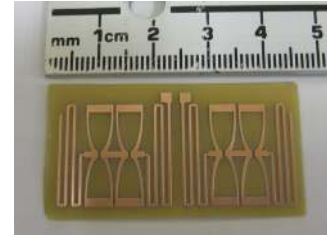


Fig. 3. Omega structure-based meander-line RFID antenna (s = 0.5 mm, k = 1.0 mm, m = 42.2 mm, a = 5.0 mm, p = 0.86 mm, $\delta$ = 4.0 mm, $\Delta$ = 18.8 mm, $\varepsilon_r$ = 3.75 (measured) and d = 0.787 mm).



Fig. 4. Measuring the tag in an anechoic chamber.

shows that ADS is an accurate tool and can be used to model the printed antennas investigated in this paper. Therefore, because of the large number of different designs in the following sections, ADS will be used exclusively to determine the characteristics of the novel designs. It should also be noted, that a passive RFID integrated circuit (IC) was attached to the ports of the antenna in Fig. 3 and the performance (i.e., experimental read range) of this tag was determined in an anechoic chamber (Fig. 4). The read range was 4.5 m and was comparable to commercially available tags that were twice as large.

## C. Results for Various Values of Substrate Permittivity

The next step is to determine the characteristics of the layout in Fig. 3 (or Fig. 1) for various values of substrate permittivity. The results from these simulations are shown in Figs. 6 - 8 for various values of $\varepsilon_r$.
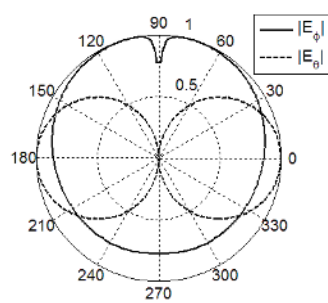
The results in Figs. 6 and 7 show that the radiation resistance increases and the resonant frequency decreases for larger values of $\varepsilon_r$. Figure 8 shows that the gain is only slightly reduced for higher values of $\varepsilon_r$. This is desirable, because
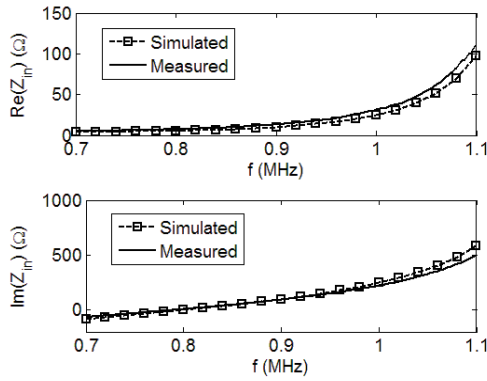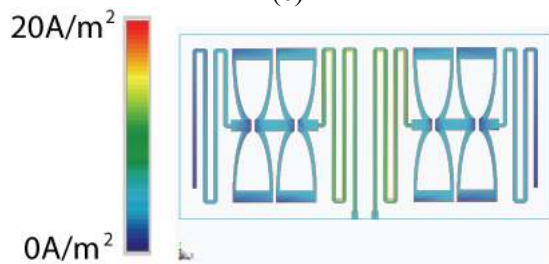
(a)
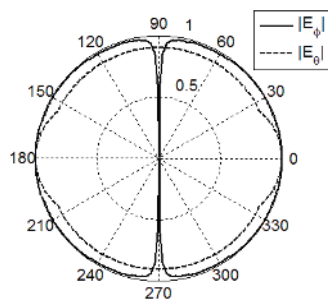


(b)



(c)



(d)

Fig. 5.    (a)  Measured  and  simulated  input
impedance  of  a  deformed  omega  structure-based
meander-line  RFID  antenna;  (b)  simulated  pattern
in the y-z plane; (c) simulated pattern in the x-z
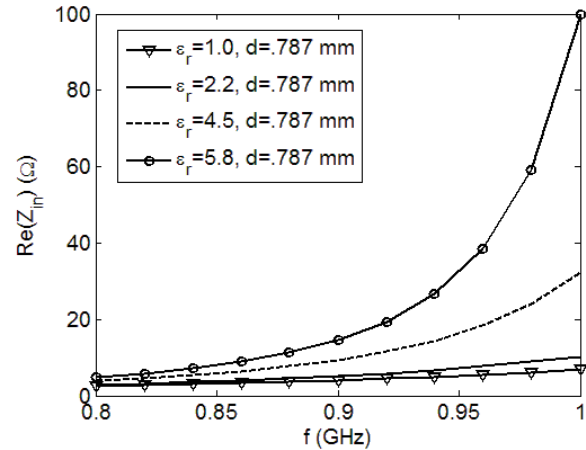plane; (d) simulated surface current at 920 MHz.



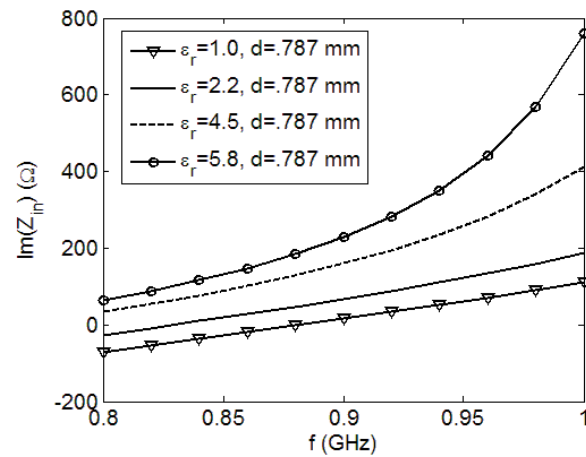Fig. 6. Input resistance of the omega structure for
various values of $\varepsilon_r$.



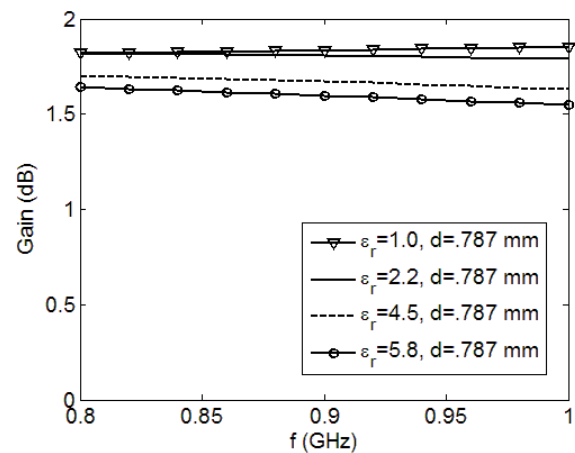Fig. 7. Input reactance of the omega structure for
various values of $\varepsilon_r$.



Fig. 8. Gain of the omega structure for various
values of $\varepsilon_r$.

typically electrically small antennas are very capacitive and have a very small input resistance below resonance. By increasing $\varepsilon_r$ the antenna can obtain useful input impedance values (approximately $10+j139\ \Omega$ [6]) and the gain is only reduced slightly.

## D.  Results for Various Values of Substrate Thickness

The next step is to determine the characteristics of the layout in Fig. 3 for various values of substrate thickness d.  The results from these simulations are shown in Figs. 9 - 11 for various values of d.

The results in Fig. 9 show that the radiation resistance increases slightly for larger values of d while the results in Fig. 10 show that the input reactance can be significantly affected by d.  Fig. 11 shows that the gain is only slightly reduced for higher values of d. This is very useful information to have, especially if it is anticipated that the RFID tag will be placed on many different types of materials and thick surfaces.

## E.  Results for Various Values of Deformed Omega Elements

The next step is to determine the characteristics of the layouts in Fig. 2 (a) – (c) for various values of $\Delta$ and number of deformed omega elements N. These layouts had the following dimensions: s = 0.5 mm, k = 1.0 mm, m = 42.2 mm, a = 5.0 mm, p = 0.86 mm, $\delta$ = 4.0 mm, $\varepsilon_r$ = 2.2 and a substrate thickness of d = 0.787 mm.

The results from these simulations are shown in Figs. 12 - 14 for various values of N and $\Delta$.  The results in Fig. 12 show that the radiation resistance is reduced as more deformed omega elements are removed as well as for smaller values of $\Delta$.  In Fig. 13 it is shown that the resonant frequency is significantly reduced as deformed omega elements are added to the design and for larger values of $\Delta$. Finally, Fig. 14 shows the gain is almost unaffected by the different values of N and $\Delta$.

## F.  Discussion and Design Guidelines

Several important comments can be made about the results in Figs. 5 – 14.

1)  In Figs. 6 – 7 and 9 – 10 it is shown that the antenna resonates at a lower frequency for larger values of $\varepsilon_r$ and d, and that the input impedance can be easily controlled with $\varepsilon_r$ and d.
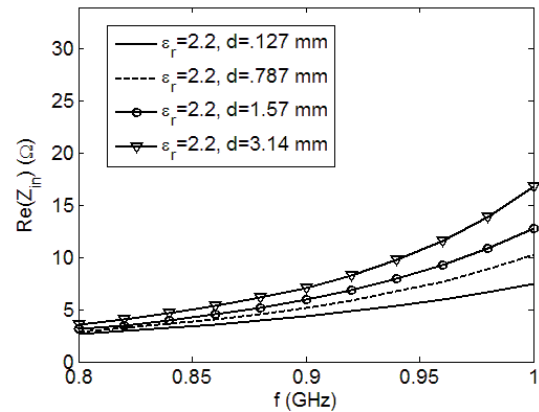


Fig. 9. Input resistance of the omega structure for various values of substrate thickness.
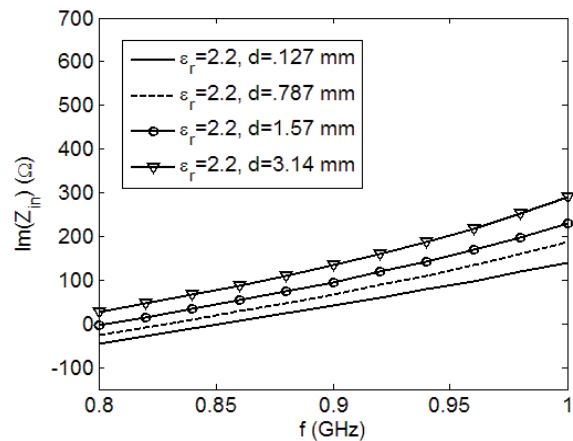


Fig. 10. Input reactance of the omega structure for various values of substrate thickness.
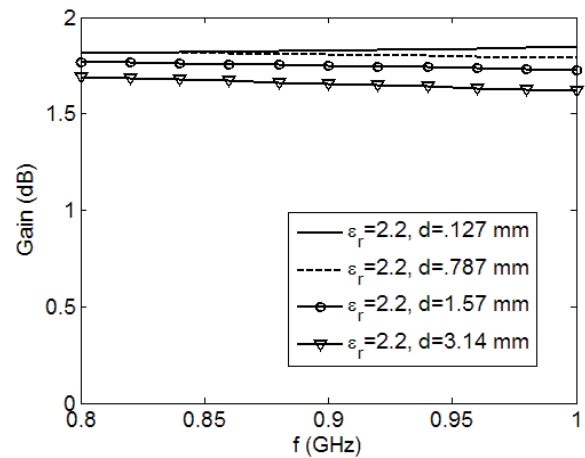


Fig. 11. Gain of the omega structure for various values of substrate thickness.
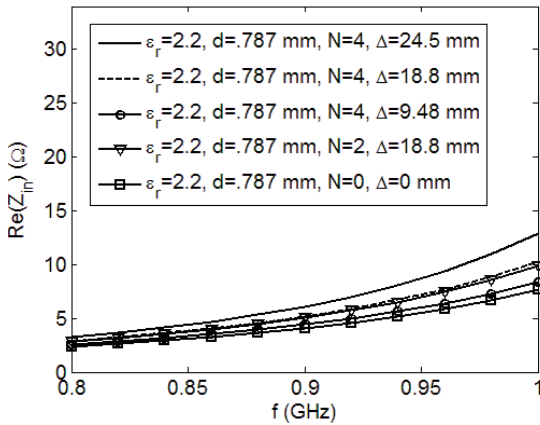
Fig. 12. Input resistance of the omega structure for various values of N and Δ for the deformed omega elements.
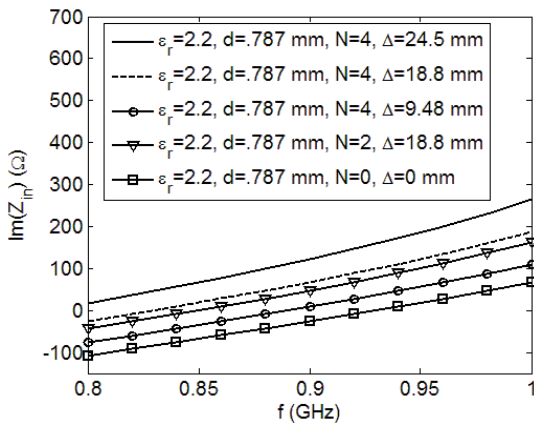


Fig. 13. Input reactance of the omega structure for various values of N and Δ for the deformed omega elements.
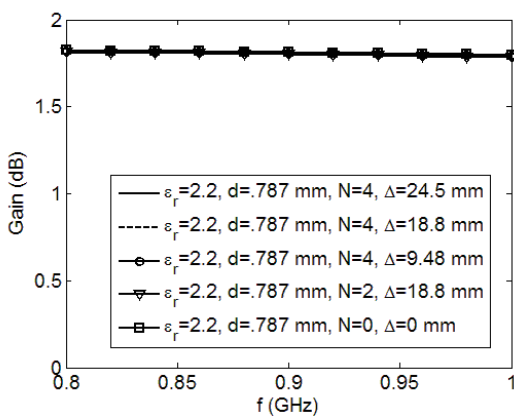


Fig. 14. Gain of the omega structure for various values of N and Δ for the deformed omega elements.

2) From the results in Figs. 12 – 13 it can be concluded that by adding more deformed omega elements to the meander-line antenna, the input resistance is only slightly changed but the resonant frequency is significantly reduced.

3) In Figs. 8, 11 and 14 it is shown that the gain is consistent for the various configurations.

4) The printed antenna design in Fig. 3 resonates at a width of m = $0.112\lambda_0$ where $\lambda_0$ the free space wavelength of the source.

5) Fig. 5 shows the largest gain is broadside to the antenna.

These results show the antenna in Fig. 1 can have many different values of input impedance while maintaining a consistent gain. This can be very useful in many design situations. Typically, when the dimensions of an antenna are changed or the antenna is placed on many different substrates, both the input impedance and gain of the antenna are significantly affected. This then requires a new design with both the input impedance and desired gain in mind. The design in Fig. 1 reduces this design effort by providing a good gain in all the cases above with flexible impedance values.

It is shown in Fig. 13 that the input impedance of the layout in Fig. 2 (b) is more inductive (i.e., resonates at a lower frequency) than the layout in Fig. 2 (a). The layout in Fig. 2 (b) is a meander-line antenna with a single deformed omega element. The impedance of each deformed omega element can be approximated as two loops with a constant current connected in parallel. This impedance can be approximated for small values of $\varepsilon_r$ with the following equation [32]:

$$ Z_a \approx \frac{1}{2} j\omega\mu_0 a \left[ \ln\left(\frac{8a}{p}\right) - 2 \right] \quad \Omega \qquad (1) $$

where a and p are defined in Fig. 1. By using (1) a designer can approximate the impact of introducing the deformed omega structure to an antenna design.

### III. SPLIT-RING RESONATOR-BASED RFID ANTENNA

The next antenna discussed is the split-ring resonator-based RFID antenna shown in Fig. 15. This antenna has two SRRs attached to each side of the RFID IC. The radius of the inner ring is denoted as r, the width of each ring is denoted as t, the gap between the rings is denoted as g, the gap on either end of the rings is denoted as w and the gap between the ports as h. For this section, the

thickness of the substrate is again denoted as d. The layout in Fig. 15 is used in all the simulations, but the dimensions are scaled and the substrate characteristics are changed to determine the behavior of the input impedance and gain of the antenna. Figure 16 (a) shows a manufactured version of the SRR antenna in Fig. 15. The magnitude of the electric field in the y-z plane is also shown in Fig. 16 (b) along with the simulated current distribution in Fig. 16 (c).

It should also be mentioned that the design in Fig. 16 a) had a max read range 1.5 m. It is anticipated that by placing the design on a substrate with a smaller value of $\varepsilon_r$, a smaller value of d and appropriate dimensions, the read range could be greatly improved.

## A. Results for Various Values of Substrate Permittivity

The next step is to determine the characteristics of the layout in Fig. 16 (a) for various values of substrate permittivity. The results from these simulations are shown in Figs. 17 - 19 for various values of $\varepsilon_r$.

The results in Fig. 17 show that the radiation resistance increases for larger values of $\varepsilon_r$ while the results in Fig. 18 show that the resonant frequency significantly reduces for larger values of $\varepsilon_r$. Figure 19 shows that the gain varies only slightly for various values of $\varepsilon_r$. The characteristics of the input impedance observed in Figs. 17 – 18 are very desirable. In particular, Fig. 18 shows that the resonance of the antenna in Fig. 16 can be below 800 MHz. This lower resonance is very significant because the antenna is resonating at an overall length that is a fraction ($q < .15\lambda_0$) of the free-space wavelength of the source. This then results in an inductive input reactance for frequencies above resonance, which are desirable for appropriate matching to RFID ICs [6], [10], [26].

## B. Results for Various Values of Substrate Thickness

The next step is to determine the characteristics of the layout in Fig. 16 (a) for various values of substrate thickness. The results from these simulations are shown in Figs. 20 - 22 for various values of d.

The results in Figs. 20 and 21 show the input impedance can be significantly affected by the substrate thickness. In particular, Fig. 21 shows the

antenna resonates at a lower frequency for thicker substrates. Similarly, the gain plot in Fig. 22 shows a larger gain is achieved for smaller values of d. Therefore, this type of antenna may be best suited for being printed on thin dielectric adhesives.
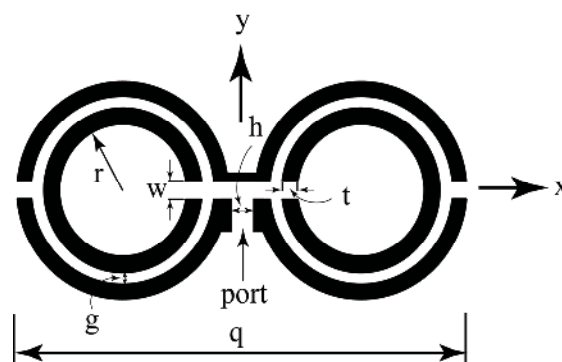


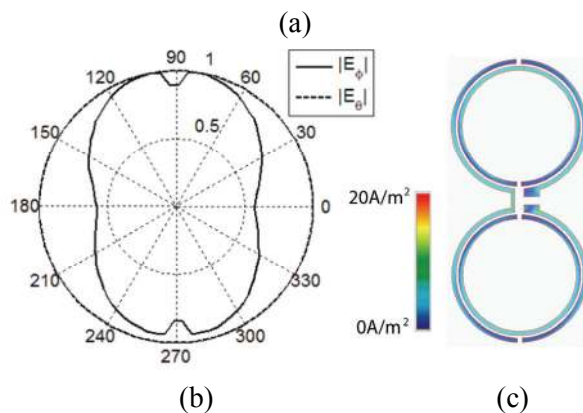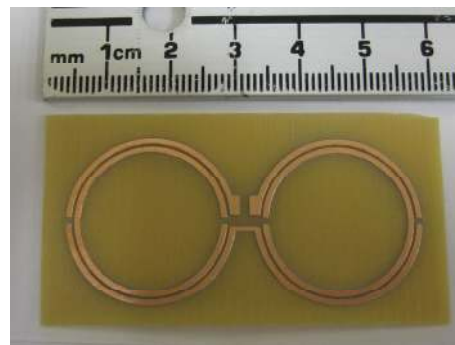Fig. 15. Dimensions of the split-ring resonator-based RFID antenna.



(a)



(b)          (c)

Fig. 16. (a) Manufactured split-ring resonator-based RFID antenna (r = 11.135 mm, t = 0.89 mm, g = 0.44 mm, q = 56.28 mm, w = 0.89 mm, h = 1.54 mm, $\varepsilon_r$ = 3.75 (measured) and d = 0.787 mm); (b) simulated pattern in the y-z plane; (c) simulated surface current at 920 MHz.

## C. Results for Various Values of r

The next step is to determine the characteristics of the layouts in Fig. 15 for various overall dimensions. This was done by scaling the following dimensions by 0.95 and 1.05: r = 11.135 mm, t = 0.89 mm, g = 0.44 mm, q = 56.28 mm, w = 0.89 mm, h = 1.54 mm and $\varepsilon_r$ = 3.75. The results from these simulations are shown in Figs. 23 - 25.

The results in Figs. 23 and 24 shows a slightly larger or smaller scale can significantly impact the input impedance. Finally, Fig. 25 shows that the gain is generally improved with a larger antenna.
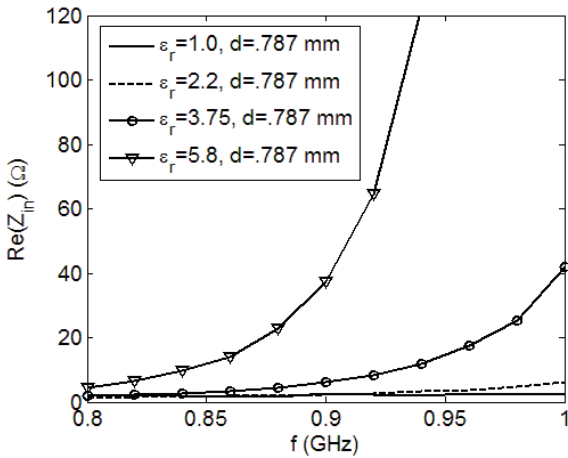

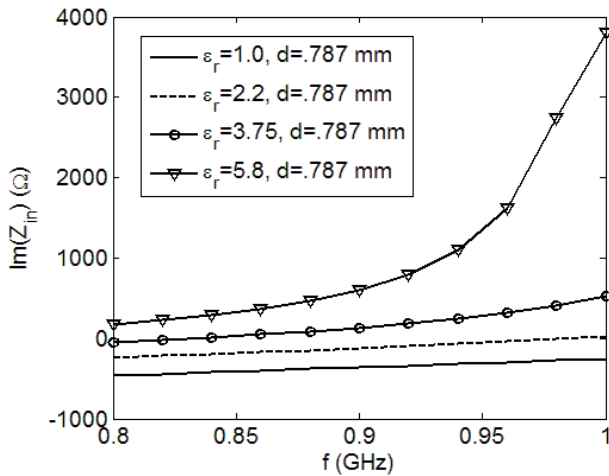
Fig. 19. Gain of the SRR structure for various values of $\varepsilon_r$.



Fig. 17. Input resistance of the SRR structure for various values of $\varepsilon_r$.



Fig. 20. Input resistance of the SRR structure for various values of substrate thickness.



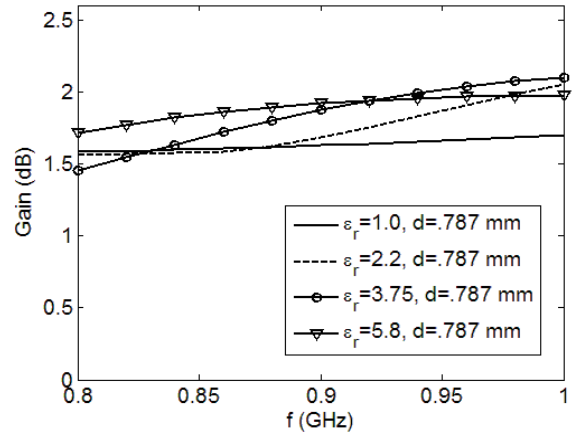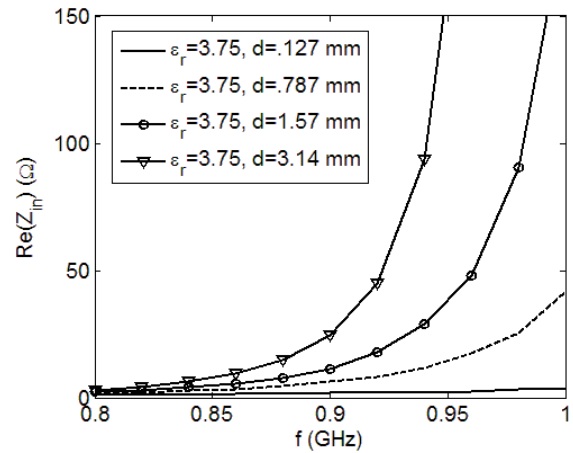Fig. 18. Input reactance of the SRR structure for various values of $\varepsilon_r$.
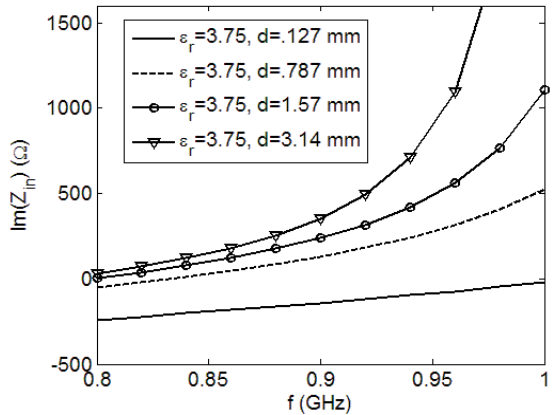


Fig. 21. Input reactance of the SRR structure for various values of substrate thickness.

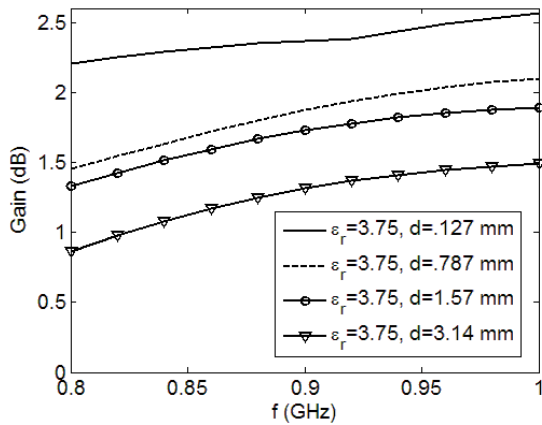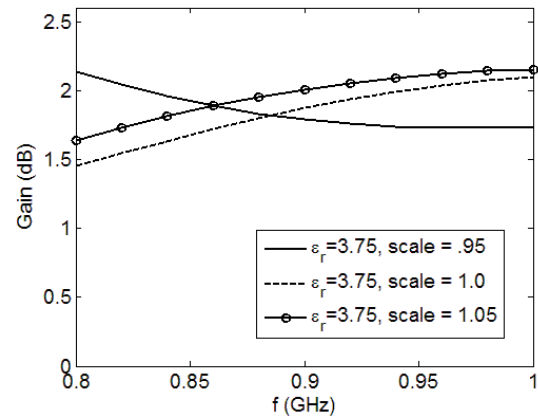Fig. 22. Gain of the SRR structure for various values of substrate thickness.



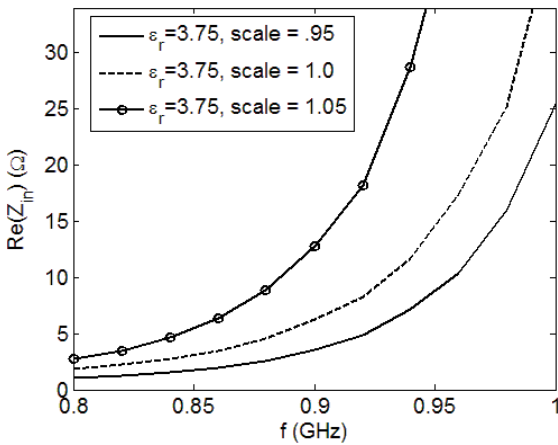Fig. 23. Input resistance of the SRR structure for various scale values.



Fig. 24. Input reactance of the SRR structure for various scale values.


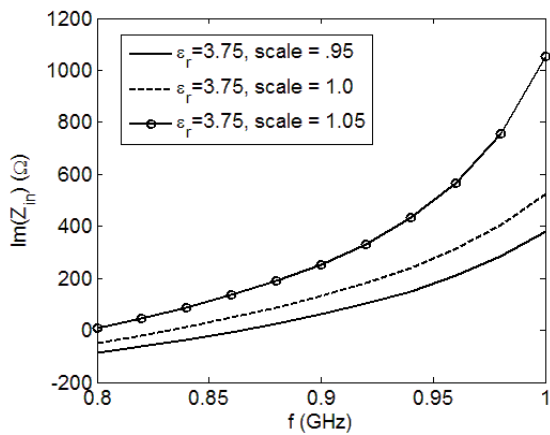
Fig. 25. Gain of the SRR structure for various scale values.

### D. Discussion and Design Guidelines

Several important comments can be made about the results in Figs. 16 – 25.

1) In Figs. 17 – 18 and 20 – 21 it is shown that the antenna resonates at a lower frequency for larger values of $\varepsilon_r$ and d, and that the input reactance can be controlled with these values.

2) In Figs. 19 and 22 it is shown that the gain of the SRR-based antenna can be significantly impacted by the larger values of $\varepsilon_r$ and d.

3) It can be concluded from Figs. 23 – 25 that scaling the antenna can affect both the gain and input impedance of the antenna.

4) The layout in Fig. 16 resonates at a width of q = $0.138\lambda_0$.

5) In Fig. 16 it is shown that the largest gain is broadside to the antenna.

The previous results show that the antenna in Fig. 15 can have many different values of input impedance and gain. In particular, Fig. 22 shows that the SRR has the largest gain for smaller dielectric substrates. This can be very useful in many design situations such as using RFID tags to track hospital records. In this situation RFID tags are placed on each individual folder of information, which can be represented as a very thin dielectric.

### IV. CONCLUSION

Two novel compact metamaterial-based antenna designs for UHF RFID tags are presented. The first design is based on a deformed omega structure found in left-handed designs and the second design is based on SRRs which are used in the designs of left-handed material. For both

designs the value of the permittivity was varied, the substrate thickness was varied and several different layouts were investigated. This resulted in a very thorough understanding of the characteristics of both designs. It has been shown that the deformed omega-based antenna is more suitable for an application on a thicker substrate while the SRR-based antenna is more suitable for applications with thin adhesive type substrates. Finally, in all cases the antennas presented here are very simple to design, very simple to manufacture, resonate at dimensions less than $0.15\lambda_0$ and are comparable to the performance of commercially available passive RFID tags with larger overall dimensions.

## ACKNOWLEDGMENTS

## REFERENCES

[1] K. Finkenzeller, *RFID Handbook: Radio-Frequency Identification Fundamentals and Applications*, John Wiley and Sons, 2002.

[2] E. Cooney, *RFID+:The Complete Review of Radio Frequency Identification*, Cengage Delmar Learning, 2006.

[3] D. Paret, R. Riesco and R. Riesco, *RFID and Contactless Smart Card Applications*, John Wiley and Sons, Inc., 2005.

[4] V. D. Hunt, A. Puglia, and M. Puglia, *RFID - A Guide to Radio Frequency Identification*, John Wiley and Sons, Inc., 2007.

[5] E. W. Schuster, S.J. Allen, and D.L. Brock, *Global RFID: The Value of the EPCglobal Network for Supply Chain Management*, Springer-Verlag New York, LLC, 2006.

[6] B. D. Braaten, G. J. Owen, D. Vaselaar, R. M. Nelson, C. Bauer-Reich, J. Glower, B. Morlock, M. Reich, and A. Reinholz, "A printed rampart-line antenna with a dielectric superstrate for UHF RFID applications,"

*IEEE International Conference on RFID,* April 16-17, 2008.

[7] M. L. Ng, K. S. Leong, D. M. Hall, and P. H. Cole, "A small passive UHF RFID tag for livestock identification," *IEEE International Symposium on Microwave, Antenna, Propagation and EMC Technologies for Wireless Communications,* vol. 1, pp. 67-70, Aug. 8-12, 2005.

[8] B. Rosenberg, *RFID: Applications, Security, and Privacy*, Pearson Education, 2006.

[9] P. Blythe, "RFID for road tolling, road-use pricing and vehicle access control," *IEE Colloquium on RFID Technology (Ref. No. 1999/123)* , pp. 811-816, Oct. 1999.

[10] K. V. S. Rao, P. V. Nikitin, and S. F. Lam "Antenna Design for UHF RFID Tags: A Review and a Practical Application," *IEEE Transactions on Antennas and Propagation,* vol. 53, no. 12, pp. 3870-3876, December 2005.

[11] H. -J. Li, H. -H. Lin, and H. -H. Wu, "Effect of antenna mutual coupling on the UHF passive RFID tag detection," *IEEE Antennas and Propagation Society International Symposium,* Jul. 2008.

[12] X. Qing and Z. N. Chen, "Proximity effects of metallic environments on high frequency RFID reader antenna: study and applications," *IEEE Transactions on Antennas and Propagation*, vol. 55, no. 11, pp. 3105-3111, Nov. 2007.

[13] R. W. Ziolkowski and C. -C. Lin, "Metamaterial-inspired magnetic-based UHF and VHF antennas," *IEEE Antennas and Propagation Society International Symposium,* July 2008.

[14] C. -J. Lee, K. M. K. H. Leong, and T. Itoh, "Composite right/left-handed transmission line based compact resonant antennas for RF module integration," *IEEE Transactions on Antennas and Propagation,* vol. 54, no. 8, pp. 2283-2291, August 2006.

[15] C. -J. Lee, K. M. K. H. Leong, and T. Itoh, "Design of resonant small antenna using composite right/left-handed transmission line," *IEEE Antennas and Propagation Society International Symposium*, pp. 218-221, July 2005.

[16] I. O. Mirza, S. Shi, C. Fazi, and D. W. Prather, "Stacked patch antenna

miniaturization using metamaterials," *IEEE Antennas and Propagation Society International Symposium,* July 2008.

[17] A. V. Kildishev and U. K. Chettiar, "Cascading optical negative index metamaterials," *ACES Journal,* vol. 22, no. 1, pp. 172-183, March 2007.

[18] A. Ali and Z. Hu, "Metamaterial resonator based wave propagation notch for ultra-wideband filter applications," *IEEE Antennas and Wireless Propagation Letters,* vol. 7, pp. 210-212, 2008.

[19] J. Bonache, M. Gil, I. Gil, J. Garcia-Garcia, and F. Martin, "On the electrical characteristics of complementary metamaterial resonators," *IEEE Microwave and Wireless Components Letters,* vol. 16, no. 10, pp. 543-545, October 2006.

[20] N. T. Messiha, A. M. Ghuniem, and H. M. El-Hennawy, "Planar transmission line medium with negative refractive index based on complementary omega-like structure", *IEEE Microwave and Wireless Components Letters,* vol. 18, no. 9, pp. 575-577, September 2008.

[21] G. V. Eleftheriades, "Analysis of bandwidth and loss in negative-refractive-index transmission-line (NRI-TL) media using coupled resonators", *IEEE Microwave and Wireless Components Letters,* vol. 17, no. 6, pp. 412-414, June 2007.

[22] G. V. Eleftheriades, "A generalized negative-refractive-index transmission-line (NRI-TL) metamaterial for dual-band and quad-band applications", *IEEE Microwave and Wireless Components Letters,* vol. 17, no. 6, pp. 415-417, June 2007.

[23] Y. -H. Ryu, J. -H. Lee, J. -Y. Kim and H.- S. Tae, "DGS dual composite right/left handed transmission line," *IEEE Microwave and Wireless Components Letters,* vol. 18, no. 7, pp. 434-436, July 2008.

[24] R. Islam and G. V. Eleftheriades, "Compact corporate power divider using metamaterial NRI-TL coupled-line couplers," *IEEE Microwave and Wireless Components Letters,* vol. 18, no. 7, pp. 440-442, July 2008.

[25] S. -G. Mao, Y. -Z. Chueh, and M. -S. Wu, "Asymmetric dual-passband coplanar waveguide filters using periodic composite right/left-handed and quarter-wavelength stubs," *IEEE Microwave and Wireless Components Letters,* vol. 17, no. 6, pp. 418-420, June 2007.

[26] J. Dacuna and R. Pous, "Miniaturized UHF tags based on metamaterials geometries," *Building Radio Frequency Identification for the Global Environment*, www.bridge-project.eu, July 2007.

[27] M. Stupf, R. Mittra, J. Yeo, and J. R. Mosig, "Some novel design for RFID antennas and their performance enhancement with metamaterials," *Microwave and Optical Technology Letters,* vol. 49, no. 4, pp. 858-867, February 2007.

[28] D. Mishra, D. R. Poddar and R. K. Mishra, "Deformed omega array as LHM," *Proceedings of the International Conference on Recent Advances in Microwave Theory and Applications*, pp. 159-160, Nov. 2008.

[29] M. Shamonin, E. Shamonina, V. Kalinin, and L. Solymar, "Resonant frequencies of a split-ring resonator: analytical solutions and numerical simulations," *Microwave and Optical Technology Letters,* vol. 44, no. 2, pp. 133-136, January 2005.

[30] K. D. Palmer and M. W. van Rooyen, "Simple broadband measurements of balanced loads using a network analyzer," *IEEE Transactions on Instrumentation and Measurement*, vol. 55, no. 1, pp. 266-272, February 2006.

[31] Agilent Technologies, *www.agilent.com*

[32] Y. Feng, B. D. Braaten, and R. M. Nelson, "Analytical expressions for small loop antennas – with application to EMC and RFID Systems," *IEEE International Symposium on Electromagnetic Compatibility*, August 2006.

**Benjamin D. Braaten** received the B.S., M.S. and Ph.D. degrees in electrical engineering from North Dakota State University, Fargo, in 2002, 2005 and 2009, respectively. He is currently an assistant professor in the electrical and computer engineering department at North Dakota State University. His research interests include antennas, radio frequency identification, complex radiation

problems, methods in computational electromagnetics, source modeling, electromagnetic compatibility and harmonic analysis.

Dr. Braaten is a member of the Applied Computational Electromagnetic Society (ACES), Institute of Electrical and Electronics Engineers (IEEE) and the national mathematics honor society Pi Mu Epsilon.

**Robert P. Scheeler** received the B.S. degree in electrical engineering at North Dakota State University, Fargo, ND in 2008. He is currently working towards the Ph.D. degree in electrical engineering at the University of Colorado at Boulder.

**Michael Reich** received the B.S. degree from North Dakota State University, Fargo, ND, in 1990, the M.S. degree from The Pennsylvania State University, State College, PA, in 1998, and the Ph.D. from North Dakota State University, Fargo, ND, in 2009, all in electrical engineering. He is currently employed by the Center for Nanoscale Science and Engineering at North Dakota State University, Fargo, ND, where he has been a Research Engineer since 2005. At the Center he has been involved in a number of projects revolving around wireless sensors, RFID systems, and antennas. He also manages the Center's RFID and Wireless Sensor Laboratory. Prior to joining the Center for Nanoscale Science and Engineering, he was employed by Phoenix International Corp. from 1997 to 2005 and by the Naval Undersea Warfare Center Division Keyport from 1990 to 1997. In these positions, he performed a wide range of activities, including embedded software development, project management, production test, and electromagnetic compatibility. His research interests include antennas (analysis, synthesis, and measurement), computational electromagnetics, RFID systems, and RF system design.

Dr. Reich is a member of the Institute of Electrical and Electronics Engineers.

**Robert M. Nelson** is currently a Professor and Program Director (of the Computer Engineering Program) at the University of Wisconsin – Stout in Menomonie, WI. Dr. Nelson received a B.A. degree in mathematics from Northland College, Ashland, WI in 1977, the M.S.E.E. degree from Washington State University, Pullman, WA in 1981, and the Ph.D. from NDSU in 1987. He has been a member of the technical staff of Bell Telephone Laboratories, has served on the faculty of the University of Idaho, and at North Dakota State University, has consulted with Michigan Technological University and Lawrence Livermore National Labs; NDSU Center for Nanoscale Science and Engineering (CNSE); Sverdrup Technology (Eglin Air Force Base); Otter Tail Power Company; and the Naval Undersea Warfare Center, New London, CT. Dr. Nelson has been working (teaching and research) in the area of applied electromagnetics, including antennas, transmission lines, microwave engineering, and EMI/EMC since 1981.

**Cherish Bauer-Reich** received the B.S. degree in physics (2003) and the M.S. degree in electrical engineering (2008) from North Dakota State University in Fargo, ND. She is currently pursuing a Ph.D. in geophysics from the University of Minnesota – Twin Cities in Minneapolis, MN. Her research interests involve modeling a wide variety of electromagnetic phenomena. She is a member of the Institute of Electrical and Electronics Engineers, American Geophysical Union, and American Physical Society.

**Jacob Glower** received the B.S., M.S. and Ph.D. degrees in electrical engineering from The Ohio State University in 1982, 1985 and 1988, respectively. He is currently an associate professor in the electrical and computer engineering department at North Dakota State University. His research interests include radio frequency identification, embedded

system design, adaptive controls and impedance controls.

**Gregory J. Owen** received the B.S. and M.S. degrees in electrical engineering at North Dakota State University, Fargo, ND in 2007 and 2009, respectively. He is currently an electrical engineer for Sebesta Blomberg and Associates in Fargo ND. His research interests include radio frequency identification, power quality and power system protection.